communications chemistry

A Nature Portfolio journal

Article

https://doi.org/10.1038/s42004-025-01589-w

Chemoproteomics identifies protein ligands for monoacylglycerol lipids

Karthik Shanbhag [1,8], Amol B. Mhetre [1,4,8], Ojal Saharan[1], Archit Devarajan [1,5,6], Anisha Rai [1,7], M. S. Madhusudhan[1,2], Harinath Chakrapani [3] ✉ & Siddhesh S. Kamat [1] ✉

Signaling lipids are important hormone-like biomolecules that regulate many physiological processes in humans. However, a significant number of them still remain poorly characterized, despite their direct association to human diseases. While the signaling pathways regulated by the endocannabinoid 2-arachidonoyl-glycerol in mammals are extensively characterized, the same cannot be said about other members of the monoacylglycerol (MAG) family of signaling lipids. Here, we report the synthesis of a bifunctional MAG probe, containing a photoreactive group and an alkyne handle. Using established chemoproteomics approaches coupled to bioorthogonal chemistry, we profile this bifunctional MAG probe in mouse brain and mammalian cell proteomes, and identify hitherto unknown protein ligands for MAG lipids. Finally, we find that the neuronal calcium sensor Hippocalcin is indeed a putative MAG protein ligand, and show that MAG lipids may have a role to play in calcium sensing and downstream signaling in the mammalian brain.

Lipids are indispensable biological building blocks that play vital roles in all forms of life. Amongst the well-known and extensively studied functions of lipids are their ability to maintain structural integrity of cells by forming hydrophobic membranes, and in energy metabolism and storage[1,2]. Besides these two conventional functions, lipids serve as precursors for the biosynthesis of steroidal hormones and are important biomarkers in the diagnosis of various human diseases, particularly metabolic disorders[1,2]. Lipids have also emerged as important signaling molecules and secondary messengers that modulate diverse biological processes, and over the past two decades, a few signaling lipid classes have been extensively investigated in the context of mammalian physiology[3]. Examples of such well-studied signaling lipids include prostaglandins[4–6], endocannabinoids[7–10], and a few classes of lysophospholipids such as sphingosine 1-phosphate[11–15], lysophosphatidic acid[16–19] and lysophosphatidylserine[20,21]. Given their importance in mammalian signaling pathways, dysregulation in their metabolism or signaling is linked to numerous human pathophysiological conditions, and drugs targeting their respective metabolic enzymes and cognate receptors are emerging as key therapies in the treatment of an array of human diseases[22,23].

The endocannabinoid 2-arachidonoyl-glycerol (2-AG) is an endogenous ligand to the cannabinoid receptors in the mammalian brain, and its metabolic and signaling pathways have been very well worked out in the mammalian nervous system[8–10,24]. Given its central role in numerous critical processes in the mammalian nervous system, modulation of 2-AG levels in the brain together with the endocannabinoid system are being rigorously explored as potential therapeutic targets for treating various neurological disorders[25–27]. 2-AG belongs to the monoacylglycerol (MAG) family of signaling lipids[8–10], and while lot is known with regards to the physiological processes regulated by 2-AG in mammals, the same cannot be said for the other MAG lipids. MAG lipids are biosynthesized from diacylglycerol (DAG) precursors by the action of the DAG lipases, and degraded by MAG lipases (Supplementary Fig. 1)[7–10]. Biologically, MAGs are known to exist in two forms, namely 1-MAG (*sn-1* MAG) and 2-MAG (*sn-2* MAG)[28], and it is speculated that these two forms of MAG can spontaneously (non-enzymatically) interconvert between each other[29]. Besides 2-AG, in vivo, MAGs are known to exist as esters of other long chain fatty acids such as palmitic acid (C16:0), oleic acid (C18:1) and linoleic acid (C18:2)[30,31], and yet little remains known of the protein ligands and the signaling pathways regulated by these (non 2-AG) MAG variants.

Coinciding with our ever-increasing knowledge of signaling lipids, over the past two decades, chemoproteomics (or chemical proteomics) has emerged as a transformative functional proteomics strategy that has enabled

[1]Department of Biology, Indian Institute of Science Education and Research, Pune, 411008 Maharashtra, India. [2]Department of Data Science, Indian Institute of Science Education and Research, Pune, 411008 Maharashtra, India. [3]Department of Chemistry, Indian Institute of Science Education and Research, Pune, 411008 Maharashtra, India. [4]Present address: Department of Pathology, University of Michigan Medical School, Ann Arbor, 48109 MI, USA. [5]Present address: New York Genome Center, New York, 10013 NY, USA. [6]Present address: Department of Biology, New York University, New York, 10013 NY, USA. [7]Present address: Department of Chemistry and Biochemistry, Georgia Institute of Technology, Atlanta, 30332 GA, USA. [8]These authors contributed equally: Karthik Shanbhag, Amol B. Mhetre. ✉e-mail: harinath@iiserpune.ac.in; siddhesh@iiserpune.ac.in

the rapid and thorough interrogation of protein-small molecule interactions on a proteome wide scale in complex biological settings[32–34]. Broadly, chemoproteomics approaches can be classified into two different categories, namely activity-based protein profiling (ABPP)[35–40], and the more recent, photoaffinity based labeling (PAL) strategy[41–45]. Traditionally, ABPP leverages the differential reactivity of amino acids (such as serine, cysteine, tyrosine) on proteins typically in enzyme active sites or ligand binding pockets[35–40]. On the other hand, the PAL strategy is non-specific in terms of amino acids, and depends almost exclusively on the binding affinity of a particular ligand to protein(s)[41–45]. While ABPP has tremendously aided the discovery and biochemical characterization of enzymes (mostly lipases) involved in the biosynthesis or degradation of signaling lipids[46,47], the PAL strategy via the development of multifunctional lipid probes has enabled the identification of protein ligands of these signaling lipids, and thus, facilitated our understanding of the biological pathways regulated by them[48].

In this study, we attempt to use the PAL strategy to identify as-of-yet unknown protein ligands for MAG lipids. Towards this, we develop a bifunctional PAL-compatible MAG probe containing a photoaffinity group and an alkyne handle. Given the physiological relevance of MAG lipids in the mammalian brain, we validate and characterize this MAG probe in the proteomic lysates of the mouse brain and a few mammalian cell lines. Next, leveraging mass spectrometry-based proteomics platforms, and using competition experiments with a control bifunctional free fatty acid probe, we identify protein ligands for MAG lipids in the mammalian nervous system. Our modeling and biochemical studies show that the calcium sensor Hippocalcin (HPCA; exclusively expressed in the central nervous system)[49,50], is indeed a protein ligand for MAG lipids, and suggests that via an interaction with HPCA, MAG lipids might have a role to play in calcium sensing and signaling pathways in mammalian brain.

Results

Development and validation of a MAG probe

In an effort to map the protein ligands of free fatty acids and establish the use of the PAL strategy for doing so, the bifunctional palmitic acid diazirine alkyne (PA-DA) probe (Fig. 1A) was developed and validated in mammalian cells using various chemoproteomics approaches[51]. We have previously described a facile two-step procedure for the synthesis of 1-MAG lipids[52], and using the PA-DA probe as the source for the free fatty acid module needed to synthesize 1-MAG lipids, we generated the 1-palmitoyl-glycerol diazirine alkyne (PG-DA) probe (Fig. 1A, Supplementary Fig. 2, Supplementary Information) at a milligram scale. Since MAG lipids are quite abundant in the central nervous system, and given our long-standing interest in identifying protein interactors for different signaling lipids in the mammalian brain, using various platforms of the PAL strategy (Supplementary Fig. 3)[42,43,48], we decided to profile the PG-DA probe in proteomic lysates generated from the mouse brain, and a few immortalized mammalian cell lines (Neuro2A, neuronal cell line; BV2, microglial cell lines; RAW264.7, macrophage cell line) that are established surrogates for different cell types in the nervous system.

To validate the photocrosslinking efficacy and downstream enrichment (using click chemistry) of putative protein targets of the PG-DA probe, first, by established gel-based chemoproteomics experiments[53] with the

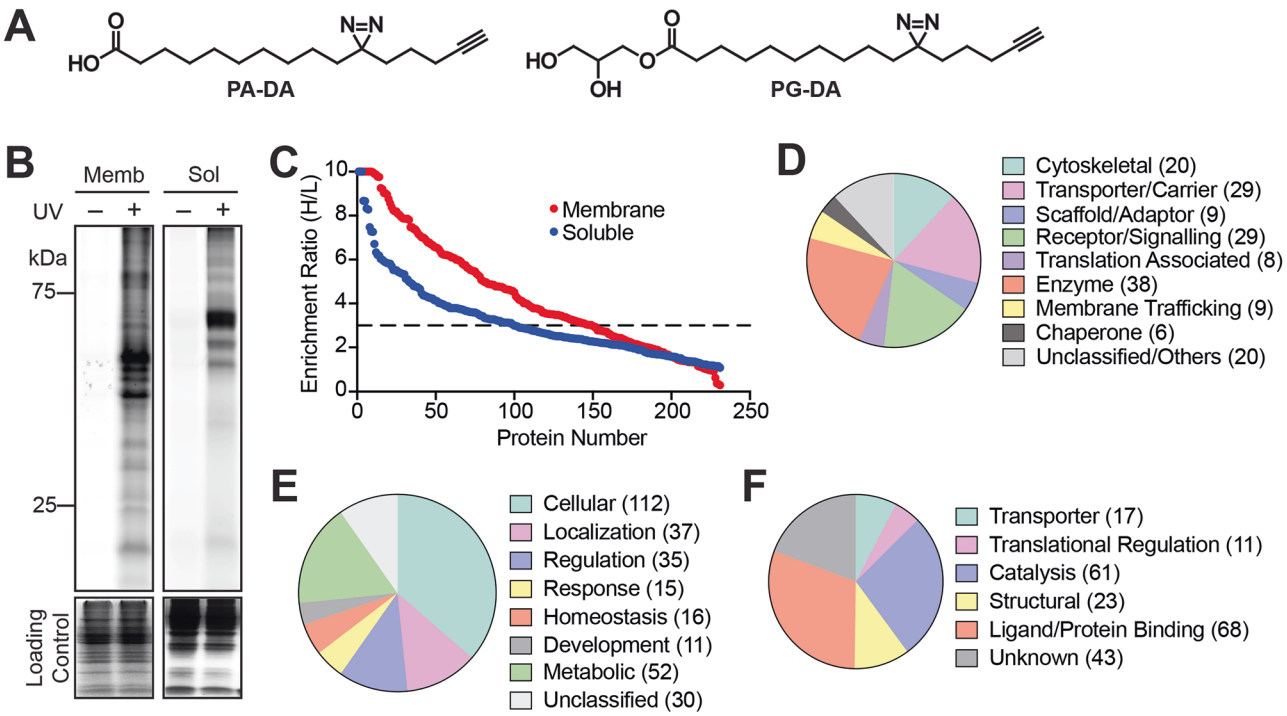

Fig. 1 | Validation of the PG-DA probe in the mouse brain proteome. A Chemical structures of the palmitic acid-diazarine-alkyne (PA-DA) and 1-palmitoyl-glycerol-diazarine-alkyne (PG-DA) probes used in this study. **B** A representative fluorescence gel from an in-gel chemoproteomics experiment showing the UV-dependent photocrosslinking of the PG-DA probe (500 μM, 6 mins of UV exposure) to proteins from the membrane (memb) and soluble (sol) proteomes prepared from the mouse brain. Coomassie staining was used to ensure equal loading in this experiment. This experiment was done three times with reproducible results each time. **C** A LC-MS/MS based chemoproteomics experiment showing enrichment ratio (heavy:light; H:L) of the total proteins identified from the UV-dependent photocrosslinking of the PG-DA probe (500 μM, 6 mins of UV exposure) from the membrane and soluble proteomes prepared from the mouse brain. Each data point represents the mean of the enrichment ratio obtained for the respective protein from two or three biological replicate for a particular proteomic fraction, based on the defined filtering criteria for this proteomics experiment. The horizontal dotted line denotes an enrichment ratio ≥ 3, and proteins having an enrichment ratio above this threshold were considered enriched by the PG-DA probe, and taken forward for subsequent analysis. Complete details for all the proteins can be found in Supplementary Data 1. **D–F** Categorization of proteins enriched by the PG-DA probe from the mouse brain proteome based on the Panther database categorization into different: (**D**) protein classes; (**E**) biological processes involved in; and (**F**) known molecular functions.

aforementioned protein lysates, we varied the ultraviolet (UV) crosslinking (irradiation) time (Supplementary Fig. 4) and probe concentration (Supplementary Fig. 5) to determine optimal conditions for subsequent experiments with the PG-DA probe. From these gel-based experiments across all the lysates tested, as expected, we found that the photocrosslinking efficacy of the PG-DA probe was UV-dependent, and the optimal probe concentration and UV crosslinking time were found to be 500 μM and 6 mins respectively (Fig. 1B, Supplementary Fig. 5). Since we wanted to use the PA-DA probe as a "control" probe in competition experiments, we decided to perform similar gel-based chemoproteomics experiments on all lysates using this probe. From this experiment, we found that the photocrosslinking of the PA-DA probe was UV-dependent, and the optimal concentration (Supplementary Fig. 6) and UV-crosslinking time (Supplementary Fig. 7) were identical to those of the PG-DA probe. Under these experimental conditions, we also looked for the intactness of both the probes across various lysates, and found by established quantitative liquid-chromatography coupled to mass spectrometry (LC-MS) analysis[54], that both probes, especially PG-DA were not degraded across all the lysates used in this study (Supplementary Fig. 8). Further, using established untargeted lipidomics analysis[54–56], we found that under our experimental conditions, neither probe was incorporated into any cellular lipid pool (e.g. phospholipids, neutral lipids etc.).

Having established optimal conditions for assaying the PG-DA probe in different lysates, next, we wanted to identify the complete repertoire of proteins enriched by it upon UV-crosslinking leveraging established LC-MS based quantitative chemoproteomics platforms[42,43,48]. In this experiment, the different lysates were treated with the PG-DA probe (500 μM, 6 mins) with or without UV-crosslinking, and the proteins enriched by the PG-DA probe upon photocrosslinking were assessed by LC-MS based quantitative chemoproteomics (Supplementary Fig. 9). For a protein to be classified as enriched by the PG-DA probe upon UV-crosslinking, it needed to be identified in at least 2 out of 3 replicates, have ≥ 3 quantified peptides per replicate, and have an enrichment ratio ≥ 3 in all replicates. Based on these filtering criteria, in the mouse brain proteome, we identified a total of 196 proteins (Fig. 1C, Supplementary Data 1), of which 94 and 46 proteins were unique to the soluble and membrane fractions respectively, while 56 proteins were identified in both proteomic fractions. Upon further categorization of the proteins enriched by the PG-DA probe from the mouse brain proteome using the PANTHER database[57,58], we found that these belonged to different types of proteins (e.g. enzymes, receptors, structural proteins, transporters, adaptors etc.) (Fig. 1D), spanned an array of biological pathways (Fig. 1E) and molecular functions (e.g. regulation, signaling, metabolism, development etc.) (Fig. 1F). Further, we found that these PG-DA enriched proteins had varied cellular localizations, with highest enrichment of cytosolic proteins, followed by membrane associated proteins that are present on mitochondria, endoplasmic reticulum, and the plasma membrane (Supplementary Fig. 10). Next, we performed similar quantitative chemoproteomics experiments with the PG-DA probe as a function of UV-crosslinking in the proteomic lysates of different mammalian cells mentioned earlier, and found relative to the results obtained from the mouse brain proteome, a comparable number of enriched proteins, having a similar spread in terms of the types of proteins enriched and their cellular localizations (Supplementary Fig. 10, 11; Supplementary Data 1). From the enriched proteins across all these experiments, we find that there are several known lipid interacting proteins, such as transporters, metabolic enzymes, signaling proteins (Supplementary Data 1). This result shows that this synthetic bifunctional lipid probe mimics the natural lipids, presumably binds to proteins in a ligand-specific manner, and hence, puts the PG-DA probe in good standing towards identifying hitherto unknown protein ligands for MAG lipids in competitive chemoproteomic experiments.

Since we aimed to use the PA-DA probe as a control in competitive chemoproteomics experiments, we also performed similar quantitative chemoproteomics experiments with this probe as a function of UV-crosslinking in the proteomic fractions of the mouse brain and the mammalian cell lines previously mentioned. Using the same criteria as that of the PG-DA probe, from these experiments, we found that the PA-DA probe also enriched a comparable number of proteins without much bias (Supplementary Fig. 12, Supplementary Data 2), and therefore, this probe could be used at similar concentrations to the PG-DA probe in the proposed competitive chemoproteomics experiments.

Competition of PG-DA versus PA-DA probe

To find the protein ligands for MAG lipids, we decided to perform a competitive chemoproteomics experiments using the PG-DA and PA-DA probes (Supplementary Fig. 13). Here, proteomes from the mouse brain or the aforementioned mammalian cell lines were incubated with the PG-DA (500 μM) or PA-DA (500 μM) probe, following which the UV-crosslinking was performed, and the proteins enriched by the respective probes in different lysates were compared using established quantitative chemoproteomics protocols[42,43,48]. For a protein to be considered for any analysis in this experiment, it needed to be identified in at least 2 out of 3 replicates, and have ≥ 3 quantified peptides per replicate. A protein was considered enriched by the PG-DA probe, if it had an enrichment ratio ≥ 1.5 in all the replicates it was identified, while an enrichment ratio ≤ 0.7 classified a protein to be enriched by the PA-DA probe. Since we were specifically interested in finding MAG interactors, we focused only on the proteins enriched by the PG-DA probe.

Based on the filtering criteria, from the experiments performed on the mouse brain proteome (Fig. 2A), we found a total of 78 proteins that were enriched by the PG-DA probe, of which, 36 and 33 proteins were found exclusively in the soluble and membrane fractions respectively, while, 9 were found in both fractions (Supplementary Data 3). From the studies performed on the lysates from different mammalian cell lines, we found that 140, 78, and 179 proteins were enriched by the PG-DA probes from the proteomes of the Neuro2A, BV2 and RAW264.7 cells respectively (Fig. 2B, Supplementary Data 3). In a quest to identify protein interactors of MAG lipids, next, we collated a list of all the proteins that were enriched by the PG-DA probe in the different lysates, and interestingly found, that the PG-DA was able to enrich 364 unique proteins that performed diverse molecular functions (Fig. 2C, Supplementary Data 3), and were involved in different biological processes (Fig. 2D, Supplementary Data 3) as per the PANTHER database categorization[57,58]. Specifically, we found that with the exception of the protein Hippocalcin (Fig. 2A) (expressed exclusively in the mammalian brain, and no other cell line)[49,50], > 350 proteins were found to be enriched by the PG-DA probe across all the different lysates tested, some of which seemed very consistent across different lysates (Supplementary Data 3). Notably, this list of enriched proteins contained known lipid interactors[53,59,60] (e.g. nucleobindin 1, fatty acid synthetase, synaptic vesicle membrane protein), thus adding confidence in the ability of the PG-DA probe to enrich putative protein ligands for MAGs.

Molecular docking studies of 1-PG in two putative MAG binding proteins

To validate the outcome of our competitive chemoproteomics experiment, and show that the PG-DA probe was able to enrich MAG-specific protein ligands, we decided to use a computational docking strategy to assess if some of the enriched proteins have hydrophobic sites or pockets capable of binding the MAG, 1-palmitoyl-glycerol (1-PG). For this experiment, we specifically chose two proteins: the neuronal calcium sensor, Hippocalcin (HPCA)[49,50], and the translocase of the outer membrane, mitochondrial import receptor subunit 22 (TOMM22)[61–63]. There were two reasons for choosing these proteins: (i) roles of MAGs in calcium sensing and mitochondrial import in the brain are poorly understood, and (ii) availability of experimentally elucidated three dimensional structures for both these proteins (PDB ID: 5G4P for human HPCA[64]; PDB ID: 7CK6 for human mitochondrial protein translocase that contains TOMM22[65]).

To determine the putative binding site of 1-PG on HPCA and TOMM22, we screened for the presence of hydrophobic pockets that could accommodate a long fatty acyl chain of 1-PG using the servers, CavityPlus[66]

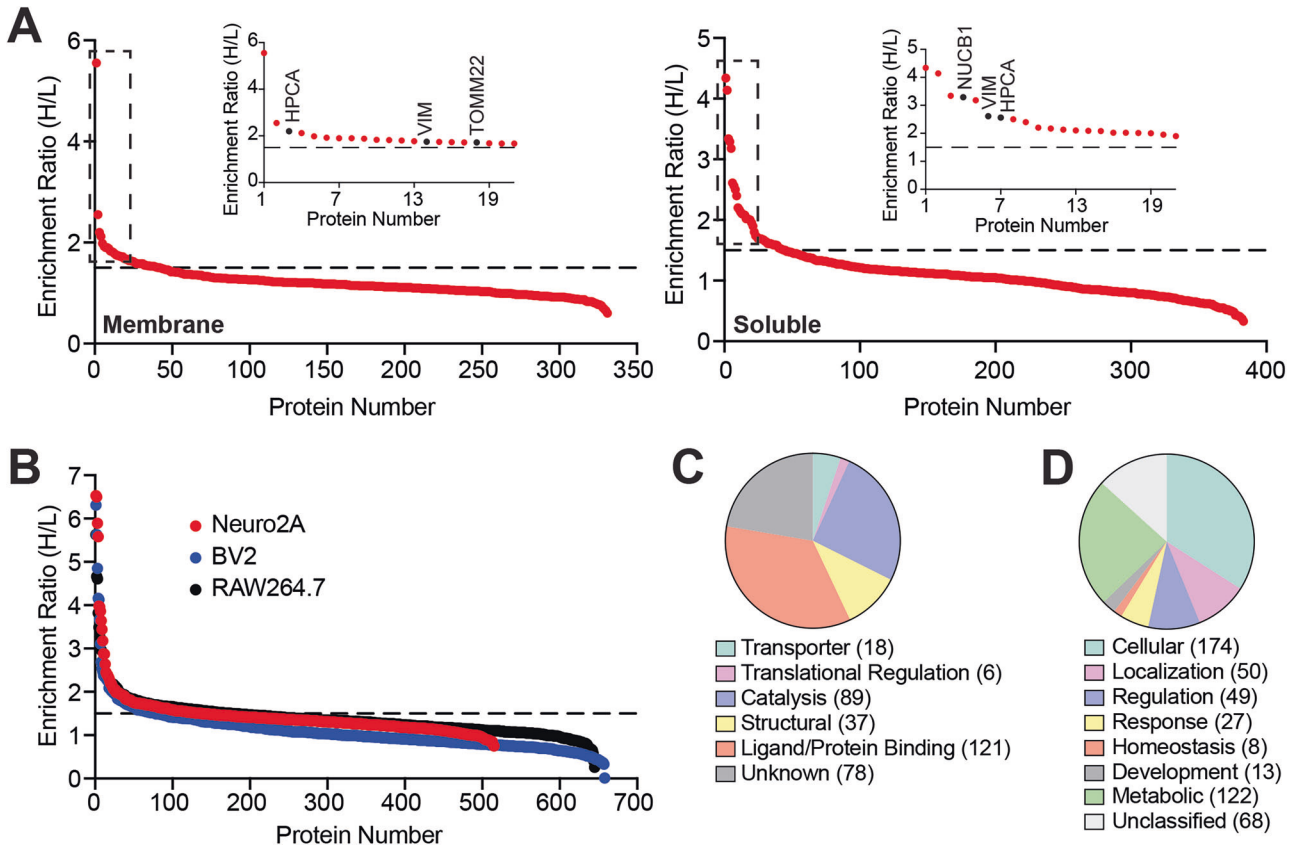

Fig. 2 | PG-DA versus PA-DA competitive chemoproteomics experiments. A, B A LC-MS/MS based proteomics analysis showing enrichment ratio (heavy:light; H:L) of the total proteins identified in this probe versus probe (PG-DA versus PA-DA) competitive chemical proteomics experiment (each probe was used at 500 μM, 6 mins of UV exposure) done with (**A**) the membrane and soluble proteomes prepared from the mouse brain; and (**B**) proteomes prepared from different immortalized mammalian cell lines (Neuro2A, BV2 and RAW264.7). Each data point in (**A**) or (**B**) represents the mean of the enrichment ratio obtained for the respective protein from two or three biological replicate for a particular proteome, based on the defined filtering criteria for this proteomics experiment. The horizontal dotted line denotes an enrichment ratio ≥ 1.5, and proteins having an enrichment ratio above this threshold were considered specifically enriched by the PG-DA probe, and taken forward for subsequent analysis. Complete details for all the proteins can be found in Supplementary Data 3. Inset in (**A**), shows high enrichment of the neuronal calcium sensor Hippocalcin (HPCA), and the mitochondrial translocase sub-unit TOMM22 by the PG-DA probe, along with known MAG interactors such as vimentin (VIM), and nucleobindin 1 (NUCB1). (**C, D**) Categorization of all the proteins specifically enriched by the PG-DA probe based on all experiments described in (**A**) and (**B**), using the Panther database categorization into different: (**C**) Known molecular functions; and (**D**) biological processes involved in.

and DEPTH[67]. Both these algorithms identified nearly identical pockets for each protein (Supplementary Fig. 14), which were further sorted based on the druggability/ligand binding score, and the cavity with the highest score and largest dimension (≥ 20 Å) was selected for the docking studies (Supplementary Fig. 14, Supplementary Data 4). Since protein-lipid interactions require hydrophobic surfaces, the electrostatics of these identified pockets were examined (Supplementary Fig. 15), and both HPCA and TOMM22 showed mostly neutral hydrophobic pockets interspersed with positive or negative charges capable of 1-PG binding. Next, we attempted to dock 1-PG in the identified hydrophobic pockets of HPCA and TOMM22 using the HADDOCK 2.4 server[68,69]. Here, the HADDOCK Score which is the weighted sum of all ligand-protein interaction energies, was used to rank and select the best cluster of generated models. For HADDOCK-ing, initially, 10,000 structures were generated for rigid body docking (it0) of which, the top 400 highest-scoring poses underwent semi-flexible refinement (it1). Subsequently, these 400 structures were subjected to final refinement step without a solvent shell (itw). The top 200 structures from this refinement step were then subjected to a RMSD-based clustering using a 1.5 Å cut-off value. Notably, the models within the best clusters for both HPCA and TOMM22, when docked with 1-PG, exhibited remarkably low standard deviations in their HADDOCK scores.

For HPCA, after the final refinement, HADDOCK categorized 183 of the 200 1-PG/HPCA complex models into 3 clusters (Supplementary Fig. 16). The best scoring cluster amongst these included 25 structures with a HADDOCK score of −35.1 ± 1.5 (RMSD = 0.25 ± 0.15 Å), wherein, 1-PG was docked into the identified hydrophobic pocket. The average van der Waals, electrostatic and ligand binding ($\Delta G_{prediction}$) energies of the top four ranked structures in this cluster were −26.4 ± 1.2 kcal/mol, −13.2 ± 2.9 kcal/mol and −8.3 ± 0.1 kcal/mol, respectively (Supplementary Data 4). Based on this docking analysis, we predict that 1-PG binds HPCA with the glycerol head situated in a positively charged region near the centre of the identified hydrophobic cavity, and the lipid tail is oriented towards the C-terminal end of the protein (Fig. 3A, Supplementary Fig. 16).

Similarly, for TOMM22, after the final refinement, 147 of 200 refined models for 1-PG and TOMM22 ligand-protein complex were sorted into 13 clusters. Since HADDOCK does not account for the presence of a lipid bilayer around the mitochondrial translocase complex, the best scoring cluster (HADDOCK Score −37.4 ± 0.5, 8 models clustered) in this case docked 1-PG into the mitochondrial membrane, which is physically impossible. Hence, the second-best cluster, with 1-PG docked into the identified ligand binding pocket with an average HADDOCK score of −35.1 ± 1.1 (RMSD = 0.20 ± 0.13 Å) was selected for further analysis (Supplementary Fig. 17). This cluster, with 4 of the generated models had average van der Waals, electrostatic and ligand binding ($\Delta G_{prediction}$) energies of −19.4 ± 0.8 kcal/mol, −38.1 ± 8.0 kcal/mol and −8.9 ± 0.2 kcal/mol, respectively (Supplementary Data 4). 1-PG possibly binds to the same cavity (that phosphatidylcholine binds to the structure) that opens towards the mitochondrial intermembrane space, with the glycerol head oriented toward the

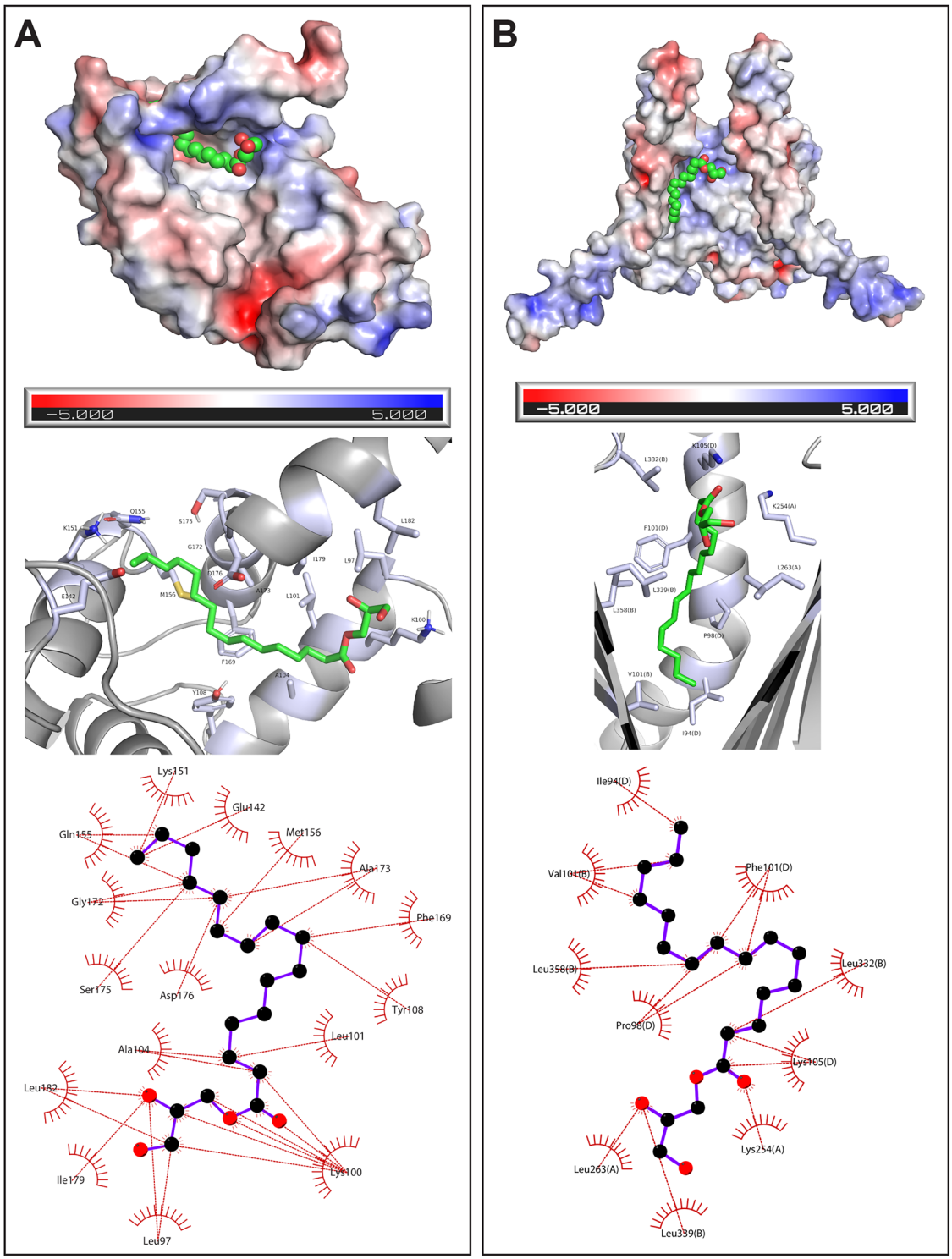

Fig. 3 | Molecular docking of 1-PG into HPCA and TOMM22. Orientation of 1-PG docked into the identified hydrophobic cavity of (**A**) HPCA and (**B**) TOMM22. In both (**A**) and (**B**), the top panel shows the docking of 1-PG in the hydrophobic cavity of an electrostatic surface model of the respective protein; the middle panel shows the possible residues interacting with 1-PG within this hydrophobic pocket; and the bottom panel shows a two-dimensional illustration of the various residues putatively interacting with 1-PG docked in the hydrophobic pocket.

opening of the cavity and the lipid tail entering one of the two possible hydrophobic grooves in the protein complex created by the TOMM40 and TOMM22 proteins (Fig. 3B, Supplementary Fig. 17). The proximity of the lipid tail of 1-PG is towards TOMM22 (to the photoreactive diazirine group of the PG-DA probe also) in the mitochondrial translocase complex, and this possibly explains why TOMM22 is the only component of this multiprotein complex that is enriched by the PG-DA probe. However, it is important to note that the overall mitochondrial translocase complex consists of several subunits, most of which are known to directly bind to the mitochondrial membrane lipids, including TOMM22. Hence, the enrichment of various TOMM-proteins (including TOMM22) from such PAL experiments with lipophilic probes is not a surprise.

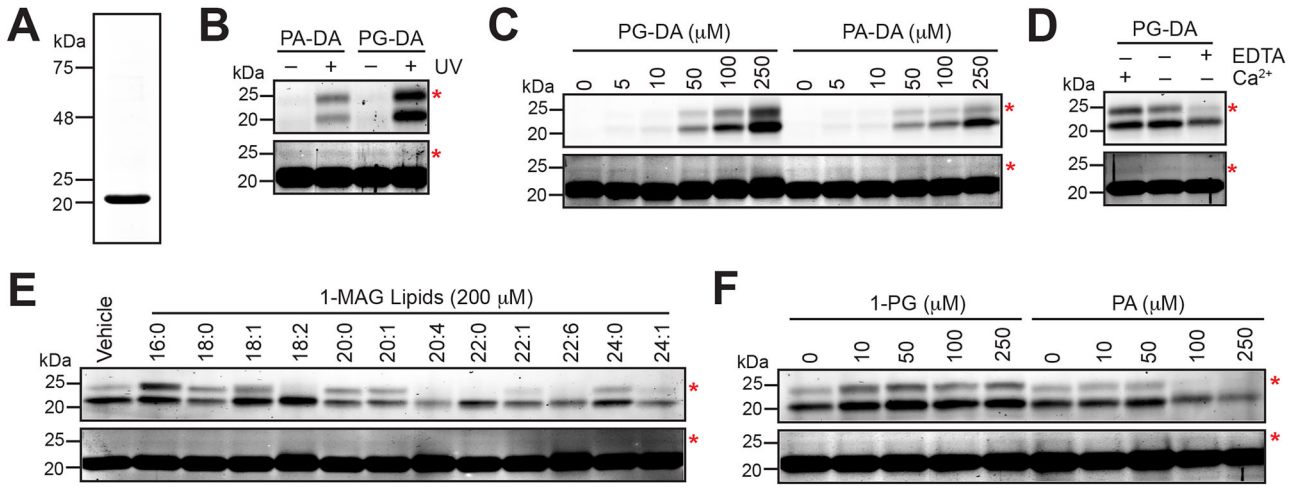

Fig. 4 | Biochemical characterization of HPCA as a putative MAG protein ligand. **A** A representative Coomassie gel showing the purity of recombinant N-terminal 6x-His tagged mouse HPCA from *E. coli* using affinity chromatography. (**B**) The UV-dependent preferential binding of the PG-DA probe to recombinantly purified mouse HPCA. In this experiment, the HPCA and lipid probe (PG-DA or PA-DA) concentrations were 10 μM and 10 μM respectively. (**C**) The dose-dependent binding of the PG-DA probe (0 – 250 μM) or the PA-DA probe (0 – 250 μM) to recombinantly purified mouse HPCA (10 μM). This experiment also shows that at comparable probe concentrations, relative to the PA-DA probe, the PG-DA probe binds much better to HPCA. (**D**) The effect of excess calcium ($CaCl_2$, 100 μM), or EDTA (100 μM) on the binding of the PG-DA probe (10 μM) to recombinantly purified mouse HPCA (10 μM). (**E**) The effect of incubating different 1-MAG variants (200 μM) on the binding of the PG-DA probe (10 μM) to recombinantly purified mouse HPCA (10 μM). (**F**) The effect of incubating increasing concentrations of 1-PG (0 – 250 μM) or PA (0 – 250 μM) on the binding of the PG-DA probe (10 μM) to recombinantly purified mouse HPCA (10 μM). For all representative gels shown in (**B–F**), the top panel shows the in-gel fluorescence, while the bottom panel is the Coomassie staining as the loading control for that respective gel. For all representative gels shown in (**B–F**), the red asterisk denotes the minor form of HPCA at 25-kDa in both gels. For all representative gels shown in (**B–F**), the Coomassie gel requires over-exposure to visualize this minor band of HPCA. For all gels shown in (**B–F**), the UV exposure time was 6 mins. All experiments shown in this figure (**A–F**), were done at least three times with reproducible results each time.

Biochemical characterization of HPCA

Having identified hydrophobic pockets in HPCA and TOMM22 capable of binding 1-PG using molecular docking approaches, next, we wanted to validate these findings biochemically. The purification of recombinant TOMM22 was fairly complicated, as this protein was not very stable and needed be purified as part of the entire mitochondrial translocase macromolecular assembly[65]. Hence, we shifted our attention towards biochemically validating HPCA using the PG-DA and PA-DA probes. We successfully expressed mouse HPCA (UniProt ID: P84075) with a N-terminal 6x-His tag in *E. coli*, and were able to purify it (>95%) using affinity chromatography (Fig. 4A). Next, we incubated the purified mouse HPCA (10 μM) with the PG-DA or PA-DA probe (10 μM, 30 min) at 37 °C, and assessed the ability of the bifunctional lipid probes to bind to purified HPCA as a function of UV-crosslinking (6 min at 37 °C). Consistent with the PG-DA versus PA-DA competition proteomics experiments (Fig. 2A), we found that the PG-DA bound significantly more to mouse HPCA than the PA-DA probe (Fig. 4B). Quite surprisingly, we found during this in-gel fluorescence experiment, the lipid probe labeled HPCA (in case of both probes) showed up as two protein bands (at ~ 20 and 25 kDa) (Fig. 4B). Upon over-exposing the loading control (Coomassie) gel (Fig. 4B), we found that HPCA was purified in two protein forms: a major form that corresponds to the 20 kDa protein, and a minor form that corresponds to the 25 kDa protein, consistent with previous reports on the purification of this protein[64]. Interestingly, we found from in-gel fluorescence experiments that the minor protein form HPCA (~ 25 kDa protein band) binds the PG-DA probe far more tightly than the major protein form (~ 20 kDa protein band) (Fig. 4B). Next, keeping the concentration of purified mouse HPCA constant (10 μM), we titrated different concentration of the PG-DA or PA-DA probe (0 – 250 μM, 30 min, 37 °C), and found from this dose-response in-gel fluorescence experiment, that at comparable concentrations, the PG-DA probe binds far more to HPCA than the PA-DA probe (Fig. 4C).

HPCA is a neuron-specific calcium sensor in the mammalian brain, and we wanted to assess the effect of PG-DA binding to HPCA as a function of calcium concentration. Given its high-affinity for calcium, recombinant HPCA is known to purify in a calcium bound state. Nonetheless, we performed an assay where purified mouse HPCA (10 μM) was first incubated with calcium (100 μM, 30 min, 37 °C) or EDTA (100 μM, 30 min, 37 °C) to chelate any bound calcium. Subsequently. these calcium surplus or devoid forms of HPCA were incubated with the PG-DA probe (10 μM, 30 min, 37 °C), to determine the binding of this lipid probe to HPCA using in-gel fluorescence. From this experiment, we found that relative to the purified HPCA, the calcium treated HPCA showed marginally more binding to the PG-DA probe than an untreated control (Fig. 4D). Counter to this, quite interestingly, we found that treating HPCA with EDTA (calcium ion chelator) resulted in a significant loss of PG-DA binding to the protein (Fig. 4D), suggesting that the binding of 1-MAGs to HPCA may be responsive to the calcium sensing function of this neuronal sensor.

Having shown the preferential binding of the PG-DA probe to purified HPCA, next, we wanted to assess if incubating HPCA with excess endogenous 1-MAG lipids could compete out this protein-probe interaction, and if there was any structure activity relationship (SAR) for this. For this, we incubated HPCA (10 μM) with a library of 1-MAG lipids (100 μM) previously synthesized by us[52], together with the PG-DA probe (10 μM, 30 min, 37 °C), and used in-gel fluorescence as a read out for this competitive chemoproteomics assay. From this SAR experiment, we found that the very-long chain fatty acid containing 1-MAG variants (chain length ≥ C20), especially those having polyunsaturated fatty acids (e.g. C20:4, C22:6) were able to efficiently compete the binding of the PG-DA probe to HPCA (Fig. 4E). On the contrary, we found that the incubation of HPCA with some long-chain fatty acid containing 1-MAGs (C16:0, C18:1), resulted in the increased binding of the PG-DA probe to HPCA (Fig. 4E). To test this premise, we incubated purified HPCA with increasing concentrations of 1-PG or palmitic acid (PA) (0 – 250 μM) in the presence of the PG-DA or PA-DA probe (10 μM, 30 min, 37 °C) to assess effect of 1-PG or PA on binding of this lipid probe to HPCA using in-gel fluorescence as a readout. Consistent with the previous SAR experiment, we found that increasing the 1-PG concentration resulted in the heightened binding of the PG-DA probe (in a dose-dependent manner from 0 – 50 μM, and constant from 50 – 250

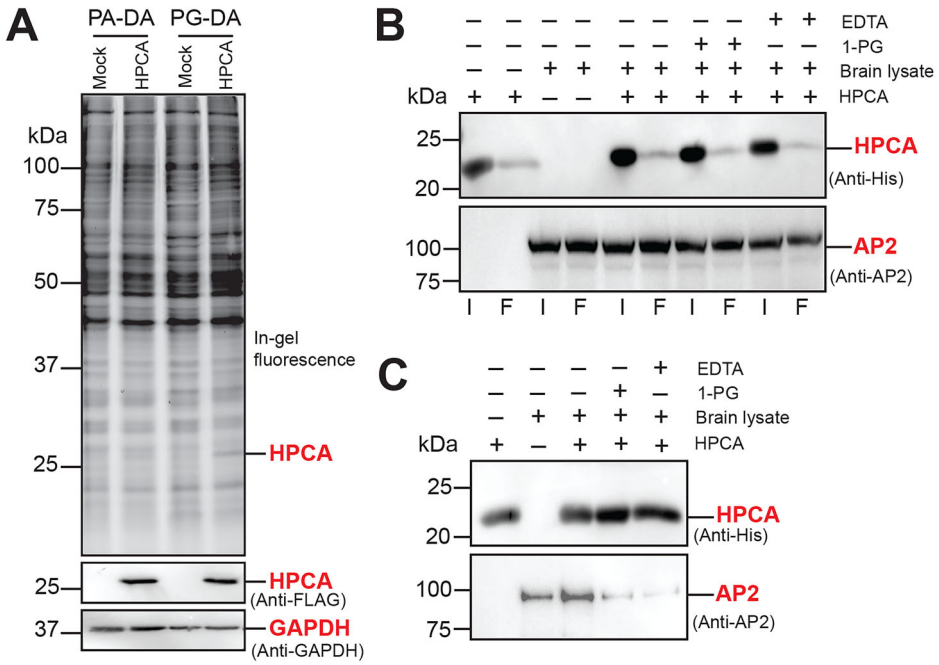

Fig. 5 | Effect of MAG on the formation of the HPCA-AP2 adaptor protein complex. A A representative in-gel fluorescence experiment showing the preferential binding of the PG-DA probe, but not the PA-DA probe, to HPCA in HEK293T cellular lysates overexpressing this protein. In this experiment, 200 µg lysates were used per condition (100 µL of 2 mg/mL), and the probes were used at 50 µM final concentration. Overexpression of HPCA in HEK293T cells was confirmed by Western blot analysis using an anti-FLAG antibody, and GAPDH was used as an equal protein loading control in this experiment. This experiment was done three times with reproducible results each time. **B** A representative Western blot image showing the Input (I) and Flow through (F) of purified HPCA (top panel) and AP2 adaptor protein from the mouse brain proteome (bottom panel) under various conditions during this immunoprecipitation experiment. From the Western blot images, as expected, a substantial portion of the recombinantly purified HPCA (6x-His tagged) is immobilized to the Ni-NTA beads, while only a small fraction of the AP2 adaptor protein from the mouse brain proteome is possibly bound to HPCA. **C** A representative Western blot image showing the elution of purified HPCA (top panel) and AP2 adaptor protein (bottom panel) from the formation of a HPCA-AP2 adaptor protein complex under various conditions during this immunoprecipitation experiment. For reasons not fully clear to us, there is some promiscuous binding of AP2 to Ni-NTA beads even in the absence of HPCA. Nonetheless, as evident from the AP2 adaptor protein elution profile from the Western blot images, the loss of calcium (from EDTA treatment) or incubation with a MAG lipid (1-PG treatment) results in substantial reduction of AP2 adaptor protein binding to HPCA. This immunoprecipitation experiment was done twice with reproducible results each time.

µM) (Fig. 4F), while increasing PA concentration resulted in the reduced binding of both probes (in a dose dependent manner) (Fig. 4F, Supplementary Fig. 18).

To establish the specificity of binding of the PG-DA probe to HPCA in complex proteomes, we overexpressed HPCA (with a N-terminal FLAG tag) in HEK293T cells using an established transient transfection protocol[52,70]. Relative to a mock transfection control, the overexpression of HPCA in the HEK293T lysates was confirmed by Western blot analysis, and both the mock and HPCA overexpressed HEK293T cellular lysates were treated with the PG-DA and PA-DA probes respectively (Fig. 5A). From this in-gel fluorescence experiment, we found that the PG-DA probe, but not PA-DA probe, was able to bind to HPCA in HEK293T lysates overexpressing this protein (Fig. 5A). As an additional control, we performed a similar in-gel fluorescence experiment on HEK293T lysates overexpressing two brain-resident lipases, ABHD12 and ABHD16A[71], and found that neither probe was able to bind to these enzymes in complex lysates (Supplementary Fig. 19). Together, these studies show that even in complex proteomes, PG-DA (and in turn 1-MAGs) show specificity in binding to HPCA.

Through established intricate cellular mechanisms[49,50,64,72–74], upon calcium binding, HPCA is known to interact with the AP2-adaptor complex at the plasma membrane. While the steps along this signaling cascade are mapped out, the role that MAG plays in this process remains unknown, and we wanted to see if MAGs had any effect on the HPCA-AP2 adaptor complex interaction. For this, we set up an immunoprecipitation (IP) assay, where His-tagged HPCA (50 µg) was immobilized on Ni-NTA beads, and brain lysates (1000 µg) were incubated with this, to investigate the HPCA-AP2 adaptor complex interaction under various conditions (Fig. 5B). Consistent with the existing mechanisms, we found that sequestration of calcium (by EDTA treatment of brain lysates) resulted in substantially diminished formation of the HPCA-AP2 adaptor complex (Fig. 5C). Quite interestingly, on similar lines, we found that incubating the brain lysates with 1-PG resulted in a similar reduction in the formation of the HPCA-AP2 adaptor complex (Fig. 5C), suggesting a possible regulatory role of MAG lipids in modulating HPCA-mediated calcium-dependent signaling in the brain. Taken together, our biochemical characterization of this neuronal sensor collectively suggests that there must be an in-built selectivity on HPCA in recognizing and binding 1-MAG lipids, which seems to be highly cooperative in nature, and is linked to the calcium-dependent signaling function of this protein.

Discussion

Over the past two decades, chemoproteomics has emerged as an invaluable tool in identifying protein ligands to numerous small bioactive molecules such as drugs, xenobiotics, and endogenous signaling molecules, and signaling lipids[32–34]. In particular, the development of synthetic strategies towards making multifunctional lipid probes in tandem with the versatility of bioorthogonal reactions has seen a steep rise in our annotation of protein ligands to a number of signaling lipids, and unraveled interesting biological pathways regulated by them[48]. Amongst the signaling lipids, given their

biomedical importance, the endocannabinoids have been extensively investigated over the years. 2-AG, an endocannabinoid, belonging to the MAG family remains the most studied member of this class of signaling lipids[8–10]. Yet interestingly, besides 2-AG, the role that other MAGs play in mammalian physiology and the proteins that they interact with remain cryptic. Recent studies have however shown that abundant non-2-AG MAGs (e.g. C16:0 MAG, C18:1 MAG) have an important role to play in glucose stimulated insulin signaling[75,76], and in the regulation of food-satiety index[77]. However, the precise mechanisms, their protein-partners, and the signaling pathways modulated by these abundant non-2-AG MAGs remain largely unknown.

To map the putative protein ligands for non-2-AG MAG lipids, here, we report the synthesis of the PG-DA probe. Initially, using in-gel fluorescence as a readout, and established chemoproteomics techniques, we successfully validate the UV-dependent photocrosslinking efficiency of this bifunctional C16:0 MAG probe, along with the previously reported PA-DA probe, in complex proteomes from the mouse brain and different immortalized mammalian cell lines (Neuro2A, RAW264.7 and BV2) in an effort to standardize downstream protocols to use PG-DA probe in tandem with the PA-DA probe to identify as-of-yet unknown protein interactors of MAG lipids. Next, using established LC-MS/MS based chemoproteomics platforms with the aforementioned proteomes, we show that the PG-DA can enrich a significant number of proteins that belong to diverse protein families, have a variety of physiological functions and are involved in different biological pathways. Further, from elaborate competition experiments of the PG-DA probe versus PA-DA probe using advanced LC-MS/MS based chemoproteomics platforms, we identify and report protein interactors of MAG lipids in the mammalian nervous system. From these MAG protein ligands, we handpicked TOMM22 and HPCA, as putative MAG-binding proteins to validate using a molecular docking approach. Our in-silico analysis showed that both TOMM22 and HPCA possess deep hydrophobic pockets where 1-PG can bind in an energetically favorable conformation. Lastly, we recombinantly purify HPCA, and show that this neuronal calcium sensor has a strong preference to bind 1-MAGs. Our studies also suggest that HPCA's interaction with 1-MAGs likely influences its ability to bind calcium or vice versa, and that this protein perhaps has an in-built selectivity and cooperativity towards binding different 1-MAG variants.

Under basal physiological conditions HPCA is exclusively expressed in the mammalian brain, where it functions as a neuronal calcium sensor, and is predominantly localized to the cytosol (Supplementary Fig. 20)[49,50]. During synaptic activation/events, the excitation of the NMDA receptor causes an influx of calcium into neurons[78–80]. This increased intracellular calcium concentration is sensed by neuronal HPCA via its EF-hand structural domains[73], and results in the exposure of the myristoyl-group of HPCA[72,74]. This calcium-bound structurally distinct myristoylated form of HPCA then translocates to the plasma membrane, and interacts with the membrane anchored AP2-adaptor complex presumably on lipid rafts enriched with phosphoinositides[81–83]. The formation of this HPCA-AP2 adaptor protein complex promotes the endocytosis of the counter AMPA receptor leading to the induction of long-term depression in hippocampal neurons via signaling from the activation of the NMDA receptor[49,50,84]. Interestingly, another study shows that the enzymatic activity ABHD6 (a putative MAG lipase) is correlated to MAG levels in the brain, and this ABHD6 activity in turn, influences the endocytosis of AMPA receptors[85]. The available literature on this protein, together with our biochemical studies, strongly suggest that there must exist a functional crosstalk between the calcium sensing activity and MAG-binding ability of HPCA (Supplementary Fig. 20), and these cooperatively are modulating the signaling events between the NMDA-AMPA receptors in the mammalian brain. Moving forward, it will be useful to understand these neuronal mechanisms in the context of HPCA, and perhaps leverage the use of 1-MAG variants (or similar compounds) as pharmacological tools in dissecting out the detailed steps involved in this process.

Besides HPCA, we also show using in-silico analysis that TOMM22 binds 1-PG. Given this, moving forward it will be interesting to see if and how 1-MAG variants are involved in different mitochondrial functions. Additionally, our competitive proteomics experiments also identify several hitherto unknown 1-MAG protein interactors, and for most of these identified proteins, a defined biochemical function or endogenous protein ligand is lacking. Thus, our data opens up several new research avenues involving MAGs, and the tools and probes described here, can facilitate the discovery of signaling pathways modulated by MAGs in tissues other than the mammalian brain. Finally, the lipid probes described here, might also prove useful tool compounds in expanding the identification of hydrophobic pockets on protein or protein-protein interfaces, and these could be exploited as potential druggable hotspots for developing new therapeutics for various human diseases.

Materials and methods

Materials

Unless mentioned otherwise, all chemicals and reagents were purchased from Sigma-Aldrich, and all tissue culture media and consumables were purchased from HiMedia.

Mice brain harvesting

All experiments involving mice used in this study were approved by the Institutional Animal Ethics Committee at IISER Pune constituted as per the guidelines provided by the Committee for the Purpose of Control and Supervision of Experiments on Animals, Government of India (Protocol No.: IISER_Pune IAEC/2023_03/02). All mice used in this study were males from the C57Bl/6 J strain, 10 – 12 weeks of age, and housed at the National Facility for Gene Function in Health and Disease (NFGFHD) at IISER Pune. In this study, the mice were deeply anaesthetized using isoflurane, and euthanized by cervical dislocation. Subsequently, their brains were surgically harvested, split sagittally into two equal anatomical parts, washed 2x with cold sterile Dulbecco's Phosphate Buffered Saline (DPBS), transferred into a 1.5 mL microcentrifuge tube, flash frozen using liquid nitrogen, and stored at −80 °C until further use.

Mammalian cell culture

All immortalized mammalian cell lines used in this study, namely Neuro2A, RAW264.7 and BV2, were purchased from ATCC, and cultured in high glucose Dulbecco's Modified Eagle Medium (DMEM) (HiMedia; Catalog No: AL066A) supplemented with 10% (v/v) Fetal Bovine Serum (FBS) (HiMedia; Catalog No: RM1112) and 1x Penicillin-Streptomycin (HiMedia; Catalog No: A001A) at 37 °C with 5% (v/v) CO_2. To prevent activation of RAW264.7 and BV2 cells, the FBS used in this media was heat inactivated by heating at 60 °C for 45 mins. All cells were routinely stained with 4',6-diamidino-2-phenylindole (DAPI) using previously described protocols[70,86], to ensure that they were devoid of any mycoplasma contamination. All cells were grown to at least 70% confluence, after which they were harvested by scraping, washed 3x with cold sterile DPBS, pelleted in a 1.5 mL microcentrifuge tube, flash frozen in liquid nitrogen, and stored at −80 °C until further use. HPCA (with a N-terminal FLAG tag), ABHD12 and ABHD16A were overexpressed in HEK293T cells by transient transfection using PEI MAX reagent (Polysciences Inc.) as per a protocol previously reported by us[52,70,87].

Preparation of proteomic lysates

Proteomic lysates from the mouse brain and mammalian cells were prepared using previously described protocols[52,70,86] in sterile DPBS, and their concentrations were estimated using the Bradford assay[88]. To specially ensure that the PG-DA probe was intact in our experiments, the proteomic lysates were pre-treated with 2 mM phenylmethylsulfonyl fluoride (PMSF) for 45 mins at 37 °C to inactivate any resident lipases that might potentially hydrolyze the PG-DA probe.

In-gel fluorescence studies

For a typical in-gel fluorescence experiment, 100 µL of proteome (concentration 2 mg/mL) was incubated with the PG-DA or PA-DA probe

(probe concentration and time of incubation mentioned in the gels represented in the figures as per the experiment) at 37 °C with constant shaking in the dark, following which the UV-crosslinking step at 365 nm (UV-crosslinking time mentioned in the gels represented in the figures as per the experiment) was performed. After UV-crosslinking of the PG-DA or PA-DA probe, and the lysates were incubated with 11 µL of the Click reaction mixture [6 µL of Tris-(benzyltriazolylmethyl)-amine (TBTA) (Sigma; Catalog No: 678937-50MG) (1.7 mM in 4:1 DMSO: *tert*-butanol) + 2 µL $CuSO_4$ (50 mM in MilliQ water) (Avra Synthesis Pvt. Ltd.; Catalog No: ASC1746) + 2 µL Tris-(2-carboxyethyl)-phosphine (TCEP) (50 mM, freshly prepared in MilliQ water) (Sigma; Catalog No: C4706-2G) + 1 µL rhodamine-azide (10 mM in DMSO) (Sigma; Catalog No: 760765-5MG)] for 60 mins at 25 °C with constant shaking. The Click reaction was quenched by adding 33 µL of 4x SDS-PAGE loading buffer, and the samples were resolved on a 10% SDS-PAGE gel. The gel was visualized for in-gel fluorescence from probe crosslinking on an iBright 1500 gel imager (ThermoFisher Scientific).

Proteomics sample preparation and LC-MS analysis

All samples were prepared using the proteomes that were processed as described earlier. For a typical proteomics experiment, 1 mL of proteome (concentration 2 mg/mL) was incubated with the PG-DA probe (500 µM) or the PA-DA probe (500 µM) for 30 mins at 37 °C with constant shaking in the dark. Following this, the UV-crosslinking step (UV-crosslinking time mentioned as per the experiment later) was performed, and the probe treated proteomes were incubated with 110 µL of the Click reaction mixture [60 µL of TBTA (1.7 mM in 4:1 DMSO: *tert*-butanol) + 20 µL $CuSO_4$ (50 mM in MilliQ water) + 20 µL TCEP (50 mM, freshly prepared in MilliQ water) + 10 µL biotin-azide (10 mM in DMSO) (Sigma; Catalog No: 762024-25MG)] for 60 mins at 25 °C with constant shaking. Thereafter, the proteomes were denatured, reductively alkylated with iodoacetamide and digested with proteomics grade trypsin (Promega; Catalog No.: V5111) using protocols previously reported by us[70,89]. For the quantitative proteomics experiments, we used the established reductive demethylation (ReDiMe) peptide labeling strategy previously described by us[70]. In the experiments involving lipid probes in the ± UV crosslinking study, the tryptic peptides obtained from the UV-crosslinking group were labeled with heavy formaldehyde (CD_2O) (Cambridge Isotope Laboratories Inc.; Catalog No: DLM-805-20), while those from the no UV group were labeled with light formaldehyde (CH_2O) (Sigma; Catalog No: 252549-25 ML). In the experiments comparing the protein targets from PG-DA versus PA-DA, the tryptic peptides obtained from the PG-DA group were labeled with heavy formaldehyde, while those from the PA-DA group were labeled with light formaldehyde. After the ReDiMe labeling for the respective experiment, the heavy and light labeled peptides were mixed, and desalted using the established StageTip protocol[90]. All LC-MS/MS was performed on a Sciex TripleTOF6600 mass spectrometer fitted with a front-end Eksigent nano-LC 425 system using LC columns and run conditions previously reported by us[89]. Briefly, all proteomic samples were acquired using an information-dependent acquisition (IDA) mode over a $m/z = 200 - 2000$. In our experiments, a full MS survey scan was followed by the MS/MS fragmentation of the 15 most intense peptides. In all our experiments, a dynamic exclusion was also enabled (repeat count, 2; exclusion duration, 6 sec) to increase peptide coverage. Peptide identification and quantification was carried out using Protein Pilot (version 2.0.1, Sciex) using the in-built Pro-Group and Paragon algorithms against the RefSeq protein database of *Mus musculus* (Release 109, last modified on 22nd September 2020) generated by UniProt. While searching the peptides, we defined iodoacetamide alkylation of cysteine as a static modification and the oxidation of methionine and N-terminal acetylation as variable modifications. The ReDiMe algorithm was selected within Protein Pilot software for quantification of identified proteins. In all our proteomic searches, the precursor ion and MS/MS mass tolerance were set at 20 and 50 ppm, respectively, for the peptide searches. Additionally, the false discovery rate (FDR) was calculated using a decoy database search, and a stringent FDR < 1% was used to filter proteins and peptides in our experiments. In all the analysis reported in this study, a maximal cut-off ratio of 10 was imposed on the enrichment ratio (heavy label to light label) for the ReDiMe labelling experiments.

Molecular docking of 1-PG into HPCA and TOMM22

The three-dimensional structures of HPCA (PDB ID: 5G4P, UniProt: P84074) and the TOMM22 complex (PDB ID: 7CK6, UniProt: Q9NS69) were obtained from the Protein Data Bank[91]. The calcium ions from HPCA and the 1,2-distearoylphosphatidylcholine from the TOMM22 complex were removed prior to docking. Further, the TOMM22 complex was also amended to appear as a single chain for docking using the PDB-Tools web server[92]. Additionally, the coordinates for 1-PG [IUPAC: (2S)-2,3-dihydroxypropyl hexadecanoate] were also obtained from the PDB. The potential ligand binding sites in HPCA and the TOMM22 complex were identified using the CavityPlus[66] and DEPTH[67] servers with their default settings, and 1-PG was docked onto them using the HADDOCK2.4 server[68,69]. Briefly, residues identified from cavity predictions were supplied to HADDOCK to define ambiguous interactions restraints (AIRs). These AIRs, input as active and passive residues, were defined as amino acid residues whose side chains point toward the identified cavity. The list of residues used as restraints for the two proteins/complexes are as follows: for HPCA: Active residues - K151, Q155, S175; Passive residues - Y52, F64, T92, S93, W103, A104, Y108, I128, R148, G172, A173, D176; and for the TOMM22 complex: Active residues - K330/TOM40(A), K105(C), K105(D); Passive residues - W86(C), P98(C), E102(C), K105(C). The ligand (1-PG) was defined as a fully flexible active residue. 10,000 structures were generated for rigid body docking (it0) of which 400 highest-scoring poses were selected for semi-flexible refinement (it1). A 7 Å cut-off was used for defining flexible regions at the interface of ligand-protein contact. These 400 structures were then subject to final refinement without a solvent shell, and the top 200 structures were used for RMSD-based clustering with a cut-off value of 1.5 Å. Default values were used for all other parameters for protein-ligand docking. Clusters were manually inspected for ligand binding in the identified pocket, and all structures were visualized using the PyMOL software. The surface electrostatics and electrostatic potentials for HPCA and the TOMM22 complex were determined using the APBS plugin for PyMOL using the AMBER force field[93]. The ligand binding energies of 1-PG to HPCA and the TOMM22 complex were calculated using the PRODIGY-LIG web server[94], and 2D pharmacophores were visualized using LigPlot+[95].

Purification of recombinant HPCA

The mouse HPCA cDNA (Horizon Discovery; Catalog No: MMM1013-202769681) was cloned into the pET45b(+) vector, between the BamHI and XhoI restriction sites, such that the protein is eventually expressed as with a N-terminal 6x-His tag. The resulting plasmid was sequenced to ensure that the gene of interest (HPCA) was in the correct reading frame, and was transformed into *E. coli* BL21 (DE3) competent cells. A single colony was picked and grown overnight in 10 mL Luria-Bertani (LB) media containing ampicillin (final concentration of 100 µg/mL) at 37 °C with constant shaking. This primary culture was used to inoculate 1 L of the same medium, and the cells were subsequently grown at 37 °C with constant shaking (~ 180 rpm) till the OD_{600} reached ~ 0.6. At this point, the protein expression was induced by adding 1 mM isopropyl β-D-1-thiogalactopyranoside and the cells were grown overnight at 20 °C with constant shaking. Overexpression was confirmed SDS-PAGE analysis, and the cells were harvested by centrifugation at 6000 g for 20 mins at 4 °C. The resulting cell pellet (~ 3 g/L culture) was re-suspended in 50 mL of lysis buffer (50 mM Tris.HCl, 150 mM NaCl, 10 mM imidazole, 2 mM PMSF at pH 8.0), and lysed using a

probe sonicator for 20 min with 10 sec ON/OFF cycle with 60% amplitude. The resulting lysate was centrifuged at 30,000 g for 30 mins at 4 °C, and the supernatant was applied to a HisTrap FF column (Cytiva; Catalog No: 17525501) which was pre-equilibrated with the binding buffer (50 mM Tris.HCl, 150 mM NaCl, 10 mM imidazole at pH 8.0) to enrich 6x-His tagged HPCA. The protein of interest (6x-His tag HPCA) was eluted from the column using an increasing gradient of imidazole (50 to 250 mM) as per the manufacturer's instructions. The collected protein fractions were assessed by SDS-PAGE analysis, and those containing the 6x-His tagged HPCA were pooled together, and dialyzed overnight at 4 °C in 50 mM Tris.HCl (pH 8.0) using a 10-kDa molecular weight cut-off membrane (ThermoFisher; Catalog No: 68100) to get rid of excess imidazole. The resulting protein was concentrated to a final concentration of 25 mg/mL (using an Amicon Ultra-15 Centrifugal Unit, Millipore; Catalog No.: UFC901024), flash frozen using liquid nitrogen as 10 µL aliquots, and stored at −80 °C until further use. Typical protein yields were 12.5 mg of purified 6x-His tagged HPCA/L culture. All in-gel fluorescence studies 10 µM of protein was used in a final volume of 40 µL in the assay buffer (50 mM Tris.HCl at pH 8.0). All UV-crosslinking step, CLICK-reaction and its quenching were the same as described earlier. All in-gel fluorescence studies using HPCA was performed on a 12.5% SDS-PAGE gel, and imaged as described earlier.

Immunoprecipitation of HPCA and brain lysates

A 30 µL aliquot Ni-NTA beads (ThermoFisher; Catalog No: 88222) was taken into LoBind microcentrifuge tubes (Eppendorf). These beads were washed twice with binding buffer (50 mM Tris.HCl and 25 mM imidazole at pH 8.0) and pelleted by centrifuging the tubes at 700 g for 2 min. The recombinant 6x His-tagged HPCA was immobilised on these washed Ni-NTA beads by incubating 50 µg purified protein (diluted to 500 µL with binding buffer) with the beads at 4°C for 60 min with constant shaking. After this incubation, the beads were washed twice with binding buffer and centrifuged at 700 g for 2 min to pellet the beads. Further, the beads were incubated at 4°C for 3 h with constant shaking with 1000 µg of pre-cleared mouse brain proteome (in binding buffer pre-treated with 10 mM PMSF, in a final volume of 500 µL) to form the HPCA-AP2 adaptor complex. During the 3 h incubation, the mouse brain proteomes were treated with vehicle (DMSO), 1-PG (10 µM), or EDTA (10 µM) to assess various effects on the formation of the HPCA-AP2 adaptor complex. After the 3 h incubation of brain proteome with the immobilized HPCA, the Ni-NTA beads were washed twice with the binding buffer. The proteins bound to the beads were eluted by heating the beads at 95°C for 5 min with 4x SDS-PAGE loading dye (with a final concentration of SDS-PAGE loading dye to be 2x). The HPCA protein or pre-cleared brain proteome added to the beads before incubating them with the beads was collected as inputs. The supernatant obtained after incubation of HPCA protein or pre-cleared brain proteome with the beads was collected as the flow through. All protein samples (elutes, inputs and flow through) were resolved on a 10% SDS-PAGE gel, and transferred onto a PVDF membrane (GE Healthcare) using standard protocols. All western blot analysis was done using protocols previously reported by us[70,86]. The primary antibodies used in this study were the anti-beta-2 adaptin (AP2B1 subunit of the AP2 adaptor complex) Ab (rabbit IgG) (Invitrogen; Catalog No.: PA1-1066) and anti-His Ab (Mouse IgG) (Abcam; Catalog No.: ab18184) antibodies at a dilution of 1:1000. The secondary antibodies used in this study were HRP-conjugated anti-rabbit Ab (Goat IgG) (Invitrogen; Catalog No.: 31460) and HRP-conjugated anti-mouse Ab (Goat IgG) (Abcam; Catalog No.: ab6789) at a dilution of 1:10,000. All blots were developed using Immobilon Western Chemiluminescent HRP Substrate (Millipore; Catalog No.: WBKLSO500) and imaged using a Syngene G-Box Chemi-XRQ gel documentation system.

Synthesis of PA-DA and PG-DA

Complete details of the synthesis of PA-DA and PG-DA, along with complete compound characterization data can be found in the Supplementary Information.

Reporting summary

Further information on research design is available in the Nature Portfolio Reporting Summary linked to this article.

Data availability

All data that supports the findings of this study are available in the paper and its associated Supporting Information or are available from Siddhesh S. Kamat upon reasonable request. All raw data from the proteomics experiments are available on the PRIDE database with accession numbers: PXD051332 (PG-DA probe ± UV), PXD051775 (PA-DA probe ± UV), and PXD051399 (PG-DA probe vs PA-DA probe competition).

Received: 11 September 2024; Accepted: 13 June 2025;
Published online: 04 July 2025

References

1. Fahy, E., Cotter, D., Sud, M. & Subramaniam, S. Lipid classification, structures and tools. *Bba-Mol. Cell Biol. L* **1811**, 637–647 (2011).
2. Sud, M. et al. LMSD: LIPID MAPS structure database. *Nucleic Acids Res* **35**, D527–D532 (2007).
3. Dennis, E. A. Lipid Cell Signaling, Enzymes, LIPID MAPS, and Mediators of Inflammation. *J. Biol. Chem.* **291**, 24431–24448 (2016).
4. Simmons, D. L., Botting, R. M. & Hla, T. Cyclooxygenase isozymes: the biology of prostaglandin synthesis and inhibition. *Pharm. Rev.* **56**, 387–437 (2004).
5. Ricciotti, E. & FitzGerald, G. A. Prostaglandins and inflammation. *Arterioscler Thromb. Vasc. Biol.* **31**, 986–1000 (2011).
6. Wymann, M. P. & Schneiter, R. Lipid signalling in disease. *Nat. Rev. Mol. Cell Biol.* **9**, 162–176 (2008).
7. Lu, H. C. & Mackie, K. An introduction to the endogenous cannabinoid system. *Biol. Psychiatry* **79**, 516–525 (2016).
8. Pacher, P., Batkai, S. & Kunos, G. The endocannabinoid system as an emerging target of pharmacotherapy. *Pharm. Rev.* **58**, 389–462 (2006).
9. Fowler, C. J. et al. The endocannabinoid signaling system: pharmacological and therapeutic aspects. *Pharm. Biochem Behav.* **81**, 248–262 (2005).
10. Di Marzo, V., Bifulco, M. & De Petrocellis, L. The endocannabinoid system and its therapeutic exploitation. *Nat. Rev. Drug Discov.* **3**, 771–784 (2004).
11. Rosen, H. & Goetzl, E. J. Sphingosine 1-phosphate and its receptors: an autocrine and paracrine network. *Nat. Rev. Immunol.* **5**, 560–570 (2005).
12. Rosen, H. & Liao, J. Sphingosine 1-phosphate pathway therapeutics: a lipid ligand-receptor paradigm. *Curr. Opin. Chem. Biol.* **7**, 461–468 (2003).
13. Gonzalez-Cabrera, P. J., Brown, S., Studer, S. M. & Rosen, H. S1P signaling: new therapies and opportunities. *F1000Prime Rep.* **6**, 109 (2014).
14. Rosen, H., Stevens, R. C., Hanson, M., Roberts, E. & Oldstone, M. B. Sphingosine-1-phosphate and its receptors: structure, signaling, and influence. *Annu Rev. Biochem* **82**, 637–662 (2013).
15. Cyster, J. G. & Schwab, S. R. Sphingosine-1-phosphate and lymphocyte egress from lymphoid organs. *Annu Rev. Immunol.* **30**, 69–94 (2012).
16. Gardell, S. E., Dubin, A. E. & Chun, J. Emerging medicinal roles for lysophospholipid signaling. *Trends Mol. Med* **12**, 65–75 (2006).
17. Lin, D. A. & Boyce, J. A. Lysophospholipids as mediators of immunity. *Adv. Immunol.* **89**, 141–167 (2006).

18. Chun, J. Lysophospholipids in the nervous system. *Prostag Oth Lipid M* **77**, 46–51 (2005).
19. Contos, J. J. A., Ishii, I. & Chun, J. Lysophosphatidic acid receptors. *Mol. Pharm.* **58**, 1188–1196 (2000).
20. Chakraborty, A. & Kamat, S. S. Lysophosphatidylserine: A Signaling Lipid with Implications in Human Diseases. *Chem. Rev.* **124**, 5470–5504 (2024).
21. Shanbhag, K., Mhetre, A., Khandelwal, N. & Kamat, S. S. The Lysophosphatidylserines-An Emerging Class of Signalling Lysophospholipids. *J. Membr. Biol.* **253**, 381–397 (2020).
22. Kano, K., Aoki, J. & Hla, T. Lysophospholipid Mediators in Health and Disease. *Annu Rev. Pathol.* **17**, 459–483 (2022).
23. Yanagida, K. & Valentine, W. J. Druggable Lysophospholipid Signaling Pathways. *Adv. Exp. Med Biol.* **1274**, 137–176 (2020).
24. Stella, N., Schweitzer, P. & Piomelli, D. A second endogenous cannabinoid that modulates long-term potentiation. *Nature* **388**, 773–778 (1997).
25. Cristino, L., Bisogno, T. & Di Marzo, V. Cannabinoids and the expanded endocannabinoid system in neurological disorders. *Nat. Rev. Neurol.* **16**, 9–29 (2020).
26. Murataeva, N., Straiker, A. & Mackie, K. Parsing the players: 2-arachidonoylglycerol synthesis and degradation in the CNS. *Br. J. Pharm.* **171**, 1379–1391 (2014).
27. Zou, S. & Kumar, U. Cannabinoid Receptors and the Endocannabinoid System: Signaling and Function in the Central Nervous System. *Int. J. Mol. Sci.* https://doi.org/10.3390/ijms19030833 (2018).
28. Ianni, F. et al. Chiral high-performance liquid chromatography analysis of mono-, di-, and triacylglycerols with amylose- and cellulose-phenylcarbamate-based stationary phases. *J. Pharm. Biomed. Anal.* **236**, 115720 (2023).
29. Iqbal, J. & Hussain, M. M. Intestinal lipid absorption. *Am. J. Physiol. Endocrinol. Metab.* **296**, E1183–E1194 (2009).
30. Hansen, H. S. & Vana, V. Non-endocannabinoid N-acylethanolamines and 2-monoacylglycerols in the intestine. *Br. J. Pharm.* **176**, 1443–1454 (2019).
31. Kondo, S. et al. 2-Arachidonoylglycerol, an endogenous cannabinoid receptor agonist: identification as one of the major species of monoacylglycerols in various rat tissues, and evidence for its generation through CA2+-dependent and -independent mechanisms. *FEBS Lett.* **429**, 152–156 (1998).
32. Jeffery, D. A. & Bogyo, M. Chemical proteomics and its application to drug discovery. *Curr. Opin. Biotechnol.* **14**, 87–95 (2003).
33. Greenbaum, D. et al. Chemical approaches for functionally probing the proteome. *Mol. Cell Proteom.* **1**, 60–68 (2002).
34. Moellering, R. E. & Cravatt, B. F. How chemoproteomics can enable drug discovery and development. *Chem. Biol.* **19**, 11–22 (2012).
35. Niphakis, M. J. & Cravatt, B. F. Enzyme inhibitor discovery by activity-based protein profiling. *Annu Rev. Biochem* **83**, 341–377 (2014).
36. Cravatt, B. F., Wright, A. T. & Kozarich, J. W. Activity-based protein profiling: from enzyme chemistry to proteomic chemistry. *Annu Rev. Biochem* **77**, 383–414 (2008).
37. Serwa, R. & Tate, E. W. Activity-based profiling for drug discovery. *Chem. Biol.* **18**, 407–409 (2011).
38. Heal, W. P., Dang, T. H. & Tate, E. W. Activity-based probes: discovering new biology and new drug targets. *Chem. Soc. Rev.* **40**, 246–257 (2011).
39. Wright, M. H. & Sieber, S. A. Chemical proteomics approaches for identifying the cellular targets of natural products. *Nat. Prod. Rep.* **33**, 681–708 (2016).
40. Sieber, S. A. & Cravatt, B. F. Analytical platforms for activity-based protein profiling--exploiting the versatility of chemistry for functional proteomics. *Chem. Commun.* 2311-2319, (2006).
41. Forrest, I. & Parker, C. G. Proteome-wide fragment-based ligand and target discovery. *Isr. J. Chem.* **63**, e202200098 (2023).
42. Conway, L. P., Li, W. & Parker, C. G. Chemoproteomic-enabled phenotypic screening. *Cell Chem. Biol.* **28**, 371–393 (2021).
43. Parker, C. G. & Pratt, M. R. Click chemistry in proteomic investigations. *Cell* **180**, 605–632 (2020).
44. Burton, N. R., Kim, P. & Backus, K. M. Photoaffinity labelling strategies for mapping the small molecule-protein interactome. *Org. Biomol. Chem.* **19**, 7792–7809 (2021).
45. Flaxman, H. A. & Woo, C. M. Mapping the Small Molecule Interactome by Mass Spectrometry. *Biochemistry* **57**, 186–193 (2018).
46. Bachovchin, D. A. & Cravatt, B. F. The pharmacological landscape and therapeutic potential of the serine hydrolases. *Nat. Rev. Drug Discov.* **11**, 52–68 (2012).
47. Simon, G. M. & Cravatt, B. F. Activity-based proteomics of enzyme superfamilies: serine hydrolases as a case study. *J. Biol. Chem.* **285**, 11051–11055 (2010).
48. Shanbhag, K., Sharma, K. & Kamat, S. S. Photoreactive bioorthogonal lipid probes and their applications in mammalian biology. *RSC Chem. Biol.* **4**, 37–46 (2023).
49. Tzingounis, A. V., Kobayashi, M., Takamatsu, K. & Nicoll, R. A. Hippocalcin gates the calcium activation of the slow afterhyperpolarization in hippocampal pyramidal cells. *Neuron* **53**, 487–493 (2007).
50. Palmer, C. L. et al. Hippocalcin functions as a calcium sensor in hippocampal LTD. *Neuron* **47**, 487–494 (2005).
51. Hulce, J. J., Cognetta, A. B., Niphakis, M. J., Tully, S. E. & Cravatt, B. F. Proteome-wide mapping of cholesterol-interacting proteins in mammalian cells. *Nat. Methods* **10**, 259–264 (2013).
52. Joshi, A. et al. Biochemical characterization of the PHARC-associated serine hydrolase ABHD12 reveals its preference for very-long-chain lipids. *J. Biol. Chem.* **293**, 16953–16963 (2018).
53. Niphakis, M. J. et al. A global map of lipid-binding proteins and their ligandability in cells. *Cell* **161**, 1668–1680 (2015).
54. Chakraborty, A. et al. Identification of ABHD6 as a lysophosphatidylserine lipase in the mammalian liver and kidneys. *J. Biol. Chem.* **301**, 108157 (2025).
55. Talwadekar, M. et al. Metabolic transitions regulate global protein fatty acylation. *J. Biol. Chem.* **300**, 105563 (2024).
56. Kumar, K., Pazare, M., Ratnaparkhi, G. S. & Kamat, S. S. CG17192 is a phospholipase that regulates signaling lipids in the gut upon infection. *Biochemistry* **63**, 3000–3010 (2024).
57. Thomas, P. D. et al. PANTHER: Making genome-scale phylogenetics accessible to all. *Protein Sci.* **31**, 8–22 (2022).
58. Mi, H., Muruganujan, A. & Thomas, P. D. PANTHER in 2013: modeling the evolution of gene function, and other gene attributes, in the context of phylogenetic trees. *Nucleic Acids Res* **41**, D377–D386 (2013).
59. Haberkant, P. et al. In vivo profiling and visualization of cellular protein-lipid interactions using bifunctional fatty acids. *Angew. Chem. Int Ed. Engl.* **52**, 4033–4038 (2013).
60. Lum, K. M. et al. Mapping protein targets of bioactive small molecules using lipid-based chemical proteomics. *ACS Chem. Biol.* **12**, 2671–2681 (2017).
61. Su, J. Y. et al. Structural basis of Tom20 and Tom22 cytosolic domains as the human TOM complex receptors. *Proceedings of the National Academy of Sciences of the United States of America* **119**, https://doi.org/10.1073/pnas.2200158119 (2022).
62. Bellot, G. et al. TOM22, a core component of the mitochondria outer membrane protein translocation pore, is a mitochondrial receptor for the proapoptotic protein Bax. *Cell Death Differ.* **14**, 785–794 (2007).
63. Saeki, K. et al. Identification of mammalian TOM22 as a subunit of the preprotein translocase of the mitochondrial outer membrane. *J. Biol. Chem.* **275**, 31996–32002 (2000).
64. Helassa, N., Antonyuk, S. V., Lian, L. Y., Haynes, L. P. & Burgoyne, R. D. Biophysical and functional characterization of hippocalcin mutants responsible for human dystonia. *Hum. Mol. Genet* **26**, 2426–2435 (2017).

65. Wang, W. et al. Atomic structure of human TOM core complex. *Cell Discov.* **6**, 67 (2020).
66. Xu, Y. et al. CavityPlus: a web server for protein cavity detection with pharmacophore modelling, allosteric site identification and covalent ligand binding ability prediction. *Nucleic Acids Res* **46**, W374–W379 (2018).
67. Tan, K. P., Nguyen, T. B., Patel, S., Varadarajan, R. & Madhusudhan, M. S. Depth: a web server to compute depth, cavity sizes, detect potential small-molecule ligand-binding cavities and predict the pKa of ionizable residues in proteins. *Nucleic Acids Res* **41**, W314–W321 (2013).
68. Honorato, R. V. et al. The HADDOCK2.4 web server for integrative modeling of biomolecular complexes. *Nat. Prot.* https://doi.org/10.1038/s41596-024-01011-0 (2024).
69. Honorato, R. V. et al. Structural Biology in the Clouds: The WeNMR-EOSC Ecosystem. *Front Mol. Biosci.* **8**, 729513 (2021).
70. Kelkar, D. S. et al. A chemical-genetic screen identifies ABHD12 as an oxidized-phosphatidylserine lipase. *Nat. Chem. Biol.* **15**, 169–178 (2019).
71. Singh, S., Joshi, A. & Kamat, S. S. Mapping the Neuroanatomy of ABHD16A, ABHD12, and Lysophosphatidylserines Provides New Insights into the Pathophysiology of the Human Neurological Disorder PHARC. *Biochemistry* **59**, 2299–2311 (2020).
72. O'Callaghan, D. W. & Burgoyne, R. D. Role of myristoylation in the intracellular targeting of neuronal calcium sensor (NCS) proteins. *Biochem Soc. T* **31**, 963–965 (2003).
73. Takamatsu, K. & Noguchi, T. Hippocalcin: a calcium-binding protein of the EF-hand superfamily dominantly expressed in the hippocampus. *Neurosci. Res* **17**, 291–295 (1993).
74. Kobayashi, M., Takamatsu, K., Saitoh, S. & Noguchi, T. Myristoylation of hippocalcin is linked to its calcium-dependent membrane association properties. *J. Biol. Chem.* **268**, 18898–18904 (1993).
75. Zhao, S. et al. α/β-Hydrolase domain-6 and saturated long chain monoacylglycerol regulate insulin secretion promoted by both fuel and non-fuel stimuli. *Mol. Metab.* **4**, 940–950 (2015).
76. Zhao, S. et al. alpha/beta-Hydrolase domain-6-accessible monoacylglycerol controls glucose-stimulated insulin secretion. *Cell Metab.* **19**, 993–1007 (2014).
77. Hansen, K. B. et al. 2-Oleoyl Glycerol Is a GPR119 Agonist and Signals GLP-1 Release in Humans. *J. Clin. Endocr. Metab.* **96**, E1409–E1417 (2011).
78. Garaschuk, O., Schneggenburger, R., Schirra, C., Tempia, F. & Konnerth, A. Fractional Ca2+ currents through somatic and dendritic glutamate receptor channels of rat hippocampal CA1 pyramidal neurones. *J. Physiol.-Lond.* **491**, 757–772 (1996).
79. Schneggenburger, R., Zhou, Z., Konnerth, A. & Neher, E. Fractional contribution of calcium to the cation current through glutamate-receptor channels. *Neuron* **11**, 133–143 (1993).
80. Sobczyk, A. & Svoboda, K. Activity-dependent plasticity of the NMDA-receptor fractional Ca2+ current. *Neuron* **53**, 17–24 (2007).
81. Gaidarov, I. & Keen, J. H. Phosphoinositide-AP-2 interactions required for targeting to plasma membrane clathrin-coated pits. *J. Cell Biol.* **146**, 755–764 (1999).
82. Beacham, G. M., Partlow, E. A. & Hollopeter, G. Conformational regulation of AP1 and AP2 clathrin adaptor complexes. *Traffic* **20**, 741–751 (2019).
83. O'Callaghan, D. W., Haynes, L. P. & Burgoyne, R. D. High-affinity interaction of the N-terminal myristoylation motif of the neuronal calcium sensor protein hippocalcin with phosphatidylinositol 4,5-bisphosphate. *Biochem J.* **391**, 231–238 (2005).
84. Luthi, A. et al. Hippocampal LTD expression involves a pool of AMPARs regulated by the NSF-GluR2 interaction. *Neuron* **24**, 389–399 (1999).
85. Wei, M. P. et al. α/β-Hydrolase domain-containing 6 (ABHD6) negatively regulates the surface delivery and synaptic function of AMPA receptors. *Proc. Natl Acad. Sci. USA* **113**, E2695–E2704 (2016).
86. Rajendran, A., Vaidya, K., Mendoza, J., Bridwell-Rabb, J. & Kamat, S. S. Functional annotation of ABHD14B, an orphan serine hydrolase enzyme. *Biochemistry* **59**, 183–196 (2020).
87. Chakraborty, A. et al. Bioinformatics analysis identifies sequence determinants of enzymatic activity for the PHARC-associated lipase ABHD12. *Biochemistry* **64**, 1852–1863 (2025).
88. Bradford, M. M. A rapid and sensitive method for the quantitation of microgram quantities of protein utilizing the principle of protein-dye binding. *Anal. Biochem* **72**, 248–254 (1976).
89. Kumar, K., Mhetre, A., Ratnaparkhi, G. S. & Kamat, S. S. A Superfamily-wide Activity Atlas of Serine Hydrolases in Drosophila melanogaster. *Biochemistry* **60**, 1312–1324 (2021).
90. Rappsilber, J., Mann, M. & Ishihama, Y. Protocol for micro-purification, enrichment, pre-fractionation and storage of peptides for proteomics using StageTips. *Nat. Protoc.* **2**, 1896–1906 (2007).
91. Berman, H. M. et al. The Protein Data Bank. *Nucleic Acids Res* **28**, 235–242 (2000).
92. Jimenez-Garcia, B., Teixeira, J. M. C., Trellet, M., Rodrigues, J. & Bonvin, A. PDB-tools web: A user-friendly interface for the manipulation of PDB files. *Proteins* **89**, 330–335 (2021).
93. Jurrus, E. et al. Improvements to the APBS biomolecular solvation software suite. *Protein Sci.* **27**, 112–128 (2018).
94. Vangone, A. et al. Large-scale prediction of binding affinity in protein-small ligand complexes: the PRODIGY-LIG web server. *Bioinformatics* **35**, 1585–1587 (2019).
95. Laskowski, R. A. & Swindells, M. B. LigPlot+: multiple ligand-protein interaction diagrams for drug discovery. *J. Chem. Inf. Model* **51**, 2778–2786 (2011).

Acknowledgements

We acknowledge financial support from the Science and Engineering Research Board (SERB), Department of Science and Technology, Government of India (Grants: SB/SJF/2021-22/01 to S.S.K.; and CRG/2023/003892 to H.C.), an EMBO Young Investigator Award (to S.S.K.), Department of Biotechnology, Government of India under the BICB Centre Scheme (Grant: BT/PR40262/BTIS/137/38/2022 to IISER Pune), and the Prime Minister's Research Fellowship (graduate student fellowship to K.S. and O.S.). We thank Saddam Shekh for technical assistance and maintenance of the biological mass spectrometry facility at IISER Pune. We thank Pooja Thakral for providing the PA-DA probe that was used in the studies reported in Fig. 4B and C. All staff members of the NFGFHD at IISER Pune (supported by a grant from the Department of Biotechnology, Govt. of India; BT/INF/22/SP17358/2016) are thanked for maintaining and providing mice for this study. Members of the S.S.K. and H.C. labs at IISER Pune are thanked for providing critical comments and inputs throughout the course of this study.

Author contributions

K.S. performed all the chemical proteomics studies with assistance from O.S.; K.S. performed all the biochemical studies with assistance from A.R.; A.D. performed all the molecular docking studies with inputs from M.S.M., K.S., and S.S.K.; A.B.M., H.C. and S.S.K. designed the synthetic route for making the chemical probes; A.B.M. developed the synthetic methodology for the chemical probes; H.C., and S.S.K. conceived the project, supervised this project and acquired funding for this project. K.S., A.B.M., H.C. and S.S.K. wrote the manuscript with inputs from all authors.

Competing interests

The authors declare no competing interests

Additional information

Supplementary information The online version contains supplementary material available at https://doi.org/10.1038/s42004-025-01589-w.

Correspondence and requests for materials should be addressed to Harinath Chakrapani or Siddhesh S. Kamat.

Peer review information *Communications Chemistry* thanks Francesc-Xabier Contreras and the other, anonymous, reviewers for their contribution to the peer review of this work.